JAAS

PAPER

View Article Online
View Journal | View Issue

Cite this: *J. Anal. At. Spectrom.*, 2015, **30**, 1329

Variable aperture extraction lens for ion beam investigation in inductively coupled plasma-mass spectrometry†

Niko Kivel,*[ab] Heiko-Dirk Potthast,[a] Ines Günther-Leopold,[a] Frank Vanhaecke[b] and Detlef Günther[c]

A variable aperture was introduced into a commercially available sector field multicollector inductively coupled plasma-mass spectrometer. A diameter-variable aperture allows an *in situ* study of the radial isotopic composition within the ion beam. Additional information on the intensity distribution could be gained. The elements boron, cadmium and lead, covering a wide mass range, were investigated. In contrast to earlier experiments [Kivel *et al.*, *Spectrochimica Acta Part B: Atomic Spectroscopy*, 2012, **76**, 126–132], the current setup allows for lower element concentration levels in the samples and a drastically reduced measurement time. A significant radial dependence of the isotopic composition within the ion beam was observed for cadmium and lead, whereas for boron, such dependence could not be detected. The beam profiles however show a systematic trend towards smaller beam diameters for higher masses. Even though the beam diameter is dependent upon the mass of the ion, the transmission into the mass spectrometer can be considered almost complete. Thus, a contribution to mass discrimination by space-charge induced beam broadening and energy-selective ion transmission, at least within the boundaries studied here, can be excluded.

Received 12th May 2014
Accepted 25th February 2015

DOI: 10.1039/c4ja00150h

www.rsc.org/jaas

1 Introduction

In inductively coupled plasma-mass spectrometry (ICP-MS), the mass discrimination is not fully understood yet. Consequently, it is intensely discussed among specialists and is a matter of controversy.[1–3] Generally speaking, mass discrimination refers to the non-stoichiometric transfer of the ions from the source to the detector, thus causing a bias between measurement results and the composition of the material studied. Various scientific fields, such as geo- and cosmochemistry,[4,5] archeology[6,7] and nuclear applications like half-life determinations[8–10] or the analysis of used nuclear fuel,[11] rely on the determination of absolute isotope ratios. Especially these fields suffer strongly from instrumental mass discrimination, because it hampers the accurate determination of such isotope ratios. Less severe consequences are faced in the case of relative isotope ratio determination, because of the direct comparison of isotope ratios between the sample and reference material. However, a smaller magnitude of mass discrimination would mitigate the influence of fluctuations over time or the influence of small differences in the matrix composition of the sample and reference.

Several sources of mass discrimination have been identified in the past by, among others, Fontaine *et al.*[12] Namely, (a) sample introduction and ion generation, (b) collisions, (c) space-charge effects and (d) energy-selective ion transmission. The contribution of the ion generation process can be neglected in ICP-MS, because of the marginally small differences in the first ionization potentials. Sample introduction, however, has an impact on the expansion behavior of the plasma in the interface section of the mass spectrometer, thus changing its thermophysical properties and consequently, the impact of collisions. A recent study on the impact of the particle collisions by computational means[13] revealed a significant contribution of particle collisions to mass discrimination between the sampler and skimmer cone, as well as downstream of the skimmer. Furthermore, a radial dependence of the ion beam isotopic composition could be reproduced with a computational model. A distinction between space-charge effects and energy-selective ion transmission is problematic, since strictly speaking, both effects are energy-dependent. The space-charge effects refer to the coulombic repulsion of like charges. Such repulsive forces cause the ion beam to broaden due to the high charge density on the beam axis. The effect of beam broadening is inversely proportional to the mass of the

[a]*Paul Scherrer Institute, 5232 Villigen PSI, Switzerland. E-mail: niko.kivel@psi.ch; Tel: +41 56 310 2226*

[b]*Ghent University, Department of Analytical Chemistry, Krijgslaan 281 – S12, 9000 Ghent, Belgium*

[c]*ETH Zürich, Laboratory of Inorganic Chemistry, Vladimir-Prelog-Weg 1-5/10, 8093 Zürich, Switzerland*

† Electronic supplementary information (ESI) available. See DOI: 10.1039/c4ja00150h

projectile. During the expansion of the plasma in the interface, the ions gain almost identical velocities due to the entrainment in the neutral species driven by gas dynamics. Hence, their kinetic energy is inversely proportional to the square root of their mass. Minor differences in the velocity obtained are a result of the plasma potential. Therefore, the resulting ion beam consists of ions with mass-dependent kinetic energy. These differences in kinetic energy cause different ion trajectories and focal points in the ion optics and in turn different beam diameters. It should be noted that in sector-field mass spectrometers the latter effect is less pronounced because of the high acceleration potentials in the kV regime, opposed to differences in initial kinetic energy in the eV range. In the case of an incomplete beam transport due to an aperture allowing a fraction of the ion beam to pass only, space-charge effects and energy-selective ion transmission will contribute to mass discrimination.

In the present study, the focus is on mass discrimination processes within the earliest stage of the ion beam, directly after charge separation. The experiments conducted are an improved version of the ion implantation experiments published previously.[14] By inserting a variable aperture into the ion beam, a direct observation of the radial variation in the isotopic composition of the ion beam was possible. From the data obtained, the ion beam profile at the aperture plane could be deduced with almost unaltered extraction ion optics. This capability distinguishes the present study from those reported elsewhere, using ion deposition/implantation with modified extraction ion optics,[15–18] no ion extraction optics with *in situ* optical ion detection,[19,20] time-resolved ion cloud detection,[21,22] or a pressure probe[23] to determine the beam profile.

2 Experimental

In previous experiments,[14] a strong radial dependence of the isotopic composition within the ion beam was observed. However, the indirect approach of implanting ions with subsequent analysis by laser ablation multicollector ICP-MS, yielded poor analytical figures of merit. To mitigate this shortcoming, the experimental setup was optimized to allow a defined fraction of the ion beam to pass into the mass spectrometer only. This makes an *in situ* analysis of the transmitted fraction of the ion beam feasible, resulting in greatly improved ion yields.

2.1 Instrumental

The instrument used in this study is a nuclearized Neptune multicollector-ICP-MS unit (Thermo Scientific, Bremen, Germany). All experiments were conducted with a quartz SSI‡-spray chamber and a PFA-ST nebulizer (both from Elemental Scientific, Omaha, USA), the uptake of the nebulizer was $\simeq$60 μL min^{-1}. A conventional quartz torch with a narrow bore sapphire injector (ID = 1.5 mm) was employed. In order to operate the nebulizer at its optimal working-point, a make-up gas was introduced between the spray-chamber and injector for tuning purposes. The cone configuration consisted of a standard sampler with H-skimmer, made from aluminum (both from AHF Analysentechnik AG, Tübingen, Germany). A complete list of the operating conditions of the ICP-MS instrument and the data acquisition parameters are summarized in Table 1.

‡ Stable sample introduction.

2.2 Reagents

All solutions were prepared with high purity water obtained from a Milli-Q purification system (Millipore Corporation, Billerica, MA, USA). The acids used throughout the experiments were of supra-pure quality (Merck KGaA, Darmstadt, Germany). Stock solutions with a concentration of 1000 mg L^{-1} were purchased from Sigma-Aldrich (Sigma-Aldrich, Buchs, Switzerland). The solutions analyzed contained B, Cd and Pb in concentrations of 1 mg L^{-1} for B and Cd and 0.1 mg L^{-1} for Pb, prepared in 3% (m/m) nitric acid.

2.3 Variable aperture

The selection of the desired beam fraction was achieved by placing a variable aperture (Programm S, #94000, SAHM Feinwerktechnik GmbH, Wetzlar-Nauborn, Germany) at the base of the extraction lens. The diameter of the orifice can be adjusted in the range of 0.5–6 mm by means of a computer-controlled actuator. To achieve co-axial alignment of the aperture and the ion beam axis, the mechanism is equipped with a micromanipulation device, allowing a total lateral travel of ±1 mm on the *xy*-plane, independently of the extraction lens, perpendicular to the beam. All manipulations on the variable aperture device can be performed under vacuum conditions. The entire device is mounted on the lens stack extension, present only in the nuclearized versions of the Element 2 and Neptune instruments. This extension provides the additional space to

Table 1 Instrument settings and data acquisition parameters for the Neptune

Operation	
Forward power	1350 W
Guard electrode	Grounded
Gas flow rates:	
Cool	13.5 L min^{-1}
Auxiliary	0.8 L min^{-1}
Sample	0.9 L min^{-1}
Make-up	0.1–0.25 L min^{-1}
Injector	Sapphire ID = 1.5 mm
Spray chamber	Elemental scientific SSI
Cones:	
Sampler	Al, standard, 1.0 mm
Skimmer	Al, H-Skimmer, 0.8 mm
Data Acquisition	
Collection mode	Static
Amplifier resistor	10^{11} Ω
Amplifier rotation	Off
Resolution	$\simeq$400, low resolution
Acquisition time	4.194 s per cycle
Background	Defocus

accommodate the micro-manipulator. Even though an installation into a standard system might be feasible, a complete redesign of the micro-manipulator would be necessary. A graphical representation of the device is given in Fig. 1. The base-plate provides a guiding-frame for the *y*-plate, allowing it to move in one direction only. The base-plate itself is fixed on the extension and provides a fixture for the *y*-plate actuator. Likewise the *y*-plate hosts a frame for the *x*-plate and the respective actuator. The aperture itself is fixed in the *x*-plate together with its actuator. Due to the existing parts of the mass spectrometer (interface and lens stack extension) and the space required for the micro-manipulator, the plane of the aperture is 2.9 mm closer to the skimmer orifice than in the standard setup. Even though the micro-manipulator was kept as small as possible, the total thickness of the device needed to be 5 mm to accommodate all features. Therefore, the extraction lens was redesigned to fit into the mass spectrometer and provide almost identical electrical fields. The complete CAD-assembly is available as ESI† in the STEP-file format. These data can be imported into any modern 3D-CAD system, or studied by online-viewers such as http://www.3dvieweronline.com.

To link the actuators with the respective moving parts of the device, 2 mm steel pins with corresponding slots were used in the case of the *x*/*y*-plates. The aperture is connected with a 0.5 mm hardened steel wire to the actuator. All sliding faces, as well as the actuator pins, were lubricated with Braycote 601 EF Vacuum Grease (Castrol (Switzerland) AG, Zug, Switzerland).

As actuators for the micro-manipulator and the aperture, small-sized servo motors (Atlas Digital Servo, HP-DS09-SCD, Hyperion Europe, Hvidovre, Denmark) were used. These servo motors offer a high torque and good reproducibility in terms of positioning. They were modified in order to be compatible with vacuum environments and controlled by micro-controller circuits. Vacuum compatibility was achieved by complete disassembling of the servo motors, subsequent removal of the oil and grease and a supply of a high vacuum compatible lubricant (Braycote 601 EF) prior to reassembling. The micro-controller deployed in this study was an Arduino Uno (http://arduino.cc). The front-end software was written in Python (https://www.python.org/). Communication was established *via* a USB-connection. Electrical connections from the micro-controller to the servo motors were fed into the spectrometer through a KF-16 vacuum flange. This flange usually serves as a port for a vacuum gauge of the instrument. To accommodate the gauge and the feed-through, a KF-16 T-piece was used.

The entire aperture/micro-manipulator assembly was floating at an extraction potential of −2000 V, except for the actuators. Due to the strong potential gradient, a significant insulation had to be applied to the actuators to protect the electronics from the high-voltage. This was achieved by mounting them *via* PMMA-blocks to the device and by covering all exposed parts and cables with Kapton tape.

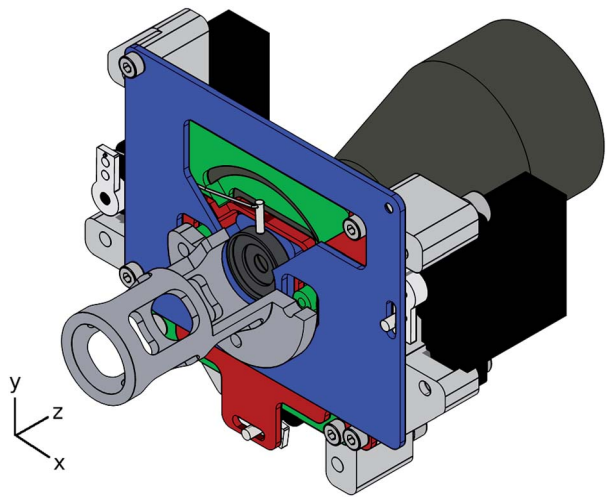

Fig. 1 Three-dimensional illustration of the variable aperture with a micro-manipulator. The micro-manipulator base-plate (green) is mounted to the lens stack extension (dark gray). The *x*-plate (blue) and *y*-plate (red) are fitted into the base-plate. The variable aperture (dark gray center) is fixed in the *x*-plate. Pins and wire levers connect the respective parts with the actuators (black) mounted around the device. Note that part of the extraction lens is cut away for better illustration.

2.4 Data acquisition procedure

The experimental procedure consisted of several tuning steps, followed by the actual data acquisition. In order to align the variable aperture and the ion beam, an orifice of 1 mm diameter was selected and the aperture was moved to the center of the assembly. The instrumental response was tuned to maximum intensity by adjusting the torch position relative to the sampler cone. After each repositioning of the torch, the make-up gas flow was optimized prior to adjusting the aperture position, the nebulizer gas flow was kept constant at all times. Several iterations of such adjustments were conducted, before adjusting the ion optics downstream of the variable aperture. The ion optics showed a strong response to *X*/*Y*-deflection, which accounts for off-axis beam positioning. Basically, the deflector bends the beam onto the entrance slit of the mass spectrometer, which is of paramount importance for reproducible measurements. After the ion optics tuning, the previous alignment steps were repeated. Yet, only negligible adjustments were necessary after the first optimization round.

Once the system was optimized to the highest intensity, the aperture was set to a large orifice (5 mm). Data were acquired for 7 blocks of 7 cycles, no outlier rejection was applied. After the successful data acquisition, the aperture was set to a smaller orifice. This process was repeated until the smallest orifice (0.5 mm) was reached. Wider step widths (0.5 mm per step) were used for large aperture diameters, steadily decreasing towards closure (0.05 mm per step).

3 Results and discussion

By using a variable aperture, the outer part of the beam can be clipped and only the central part is passing into the mass spectrometer. This direct analysis has many benefits compared to a previous setup, wherein an implantation target was studied using laser ablation MC-ICP-MS. Therefore, the analyte concentrations of the solutions analyzed could be adjusted to

the levels usually encountered in isotopic analysis. Furthermore, the time per experiment is reduced from several days for ion implantation experiments to a few hours, which mitigates the issue of potential instrumental drift during the experiment.

In the results of the ion implantation experiments published earlier,[14] no radial dependence of the isotopic composition in the ion beam could be detected for the light elements studied, lithium or boron. This was attributed to the low signal-to-noise ratio, caused by the insufficient yield of the dual step approach. To compensate for the low yield, the element concentrations in the solutions were increased to very high levels and the experiments lasted several days to accumulate sufficient amounts on the targets. This long exposure to the ion beam led to significant sputtering of the target, which compromised the determination of the beam profile. Furthermore, Chen and Farnsworth[17] reported additional complications, most importantly the likely deposition of neutral species on the target, as well as differences in the adherence to the target for certain elements.

However the implantation experiments provided direct information on the isotopic composition at a given target location, the data from the variable aperture represent the integral beam intensity I_m, with the area of the aperture A_{max} (eqn (1)).

$$I_m = \int_0^{A_{max}} f(A)\mathrm{d}A \quad (1)$$

Therefore, no *ad hoc* information of the isotopic composition at a particular position is available. In order to derive the beam intensity profile, a Weibull distribution was chosen to fit the measured data (eqn (2)),

$$f(A) = I_{sat}(1 - e^{-(\lambda A)^k}) \quad (2)$$

with A the area of the aperture, I_{sat} the saturation intensity and λ and k the scale and shape-factors, respectively. The Weibull distribution was chosen because of its high flexibility in data representation. It can act, given the proper parameters, as normal, asymmetric or exponential distribution. Because the beam intensity at a fully closed aperture can be assumed to be zero, the exponential term lacks an offset parameter, thus $\lim_{A\to 0} f(A) = 0$. The isotope ratios were derived from the intensity fits obtained and were compared to the measurements.

In the top part of Fig. 2, the results of such fitting are presented for the lead isotopes ^{206}Pb and ^{208}Pb. The typical precision of the intensity values is better than ±5%, no error-bars are given in plot to improve the readability. The correlation coefficients of the intensity fits are typically better than $R^2 \simeq 0.95$. As an additional quality criterion for the fitting, the correlation between the measured isotope ratio and the quotient of the fit-functions was also used and found to be better than $R^2 \simeq 0.95$. Considering the circumstances of a correlation between measurements and the quotient of two independent fits, with three free parameters each, this is a remarkable result. In Fig. 2 (bottom), a graphical comparison of the measured isotope ratio and the quotient of the fit-functions is given. The correlation between both datasets is 97%, the error bars represent the

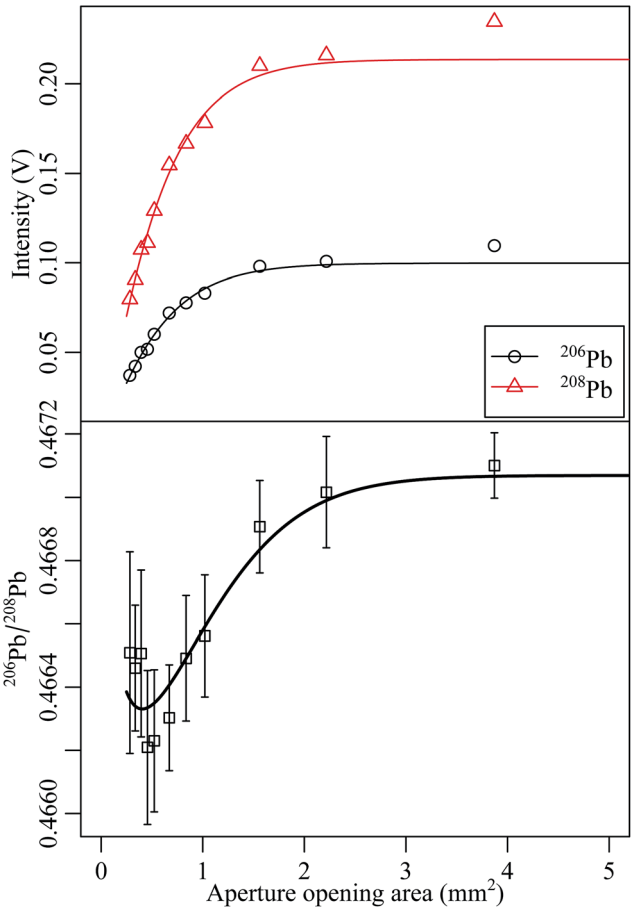

Fig. 2 Measured Pb intensity and fits of the respective data by a Weibull-distribution (top). The bottom part of the figure shows the measured ^{206}Pb/^{208}Pb isotope ratio as well as the quotient of the fit-functions.

standard deviation of the raw data ($n = 49$). In this case, raw data refer to gain factor- and decay-corrected values from the instrument software; as mentioned earlier, no outlier rejection was performed.

The same procedure was applied to the cadmium data. Fitting results for ^{110}Cd and ^{114}Cd are presented in the upper part of Fig. 3, and the measured isotope ratio with the respective fit-function ratio is given in Fig. 3 (bottom). Again a good correlation between measurement and the mathematical model is observed.

One aim of the optimized experimental setup was the higher ion yield and a simplified work-flow in order to access the light elements. For the beam intensity profile this goal was achieved (top of Fig. 4), however, no significant correlation between the isotope ratios obtained and the aperture opening was observed (bottom of Fig. 4). Even at higher ion beam intensities, a correlation between the boron isotope ratio and the aperture opening was absent. The reason for this observation remains unclear.

Due to the integral nature of the acquired data, the beam profiles cannot be gathered from the measurements without further treatment. To deduce the beam profile, at first the sum

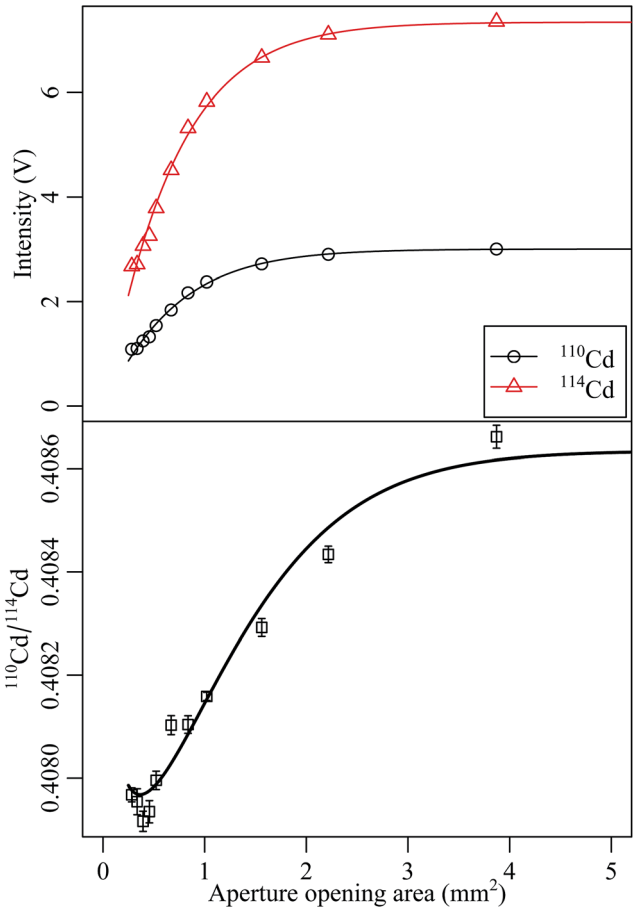

Fig. 3 Measured Cd intensity and fits of the respective data by a Weibull-distribution (top). The bottom part of the figure shows the measured ^{110}Cd/^{114}Cd isotope ratio as well as the quotient of the fit-functions.

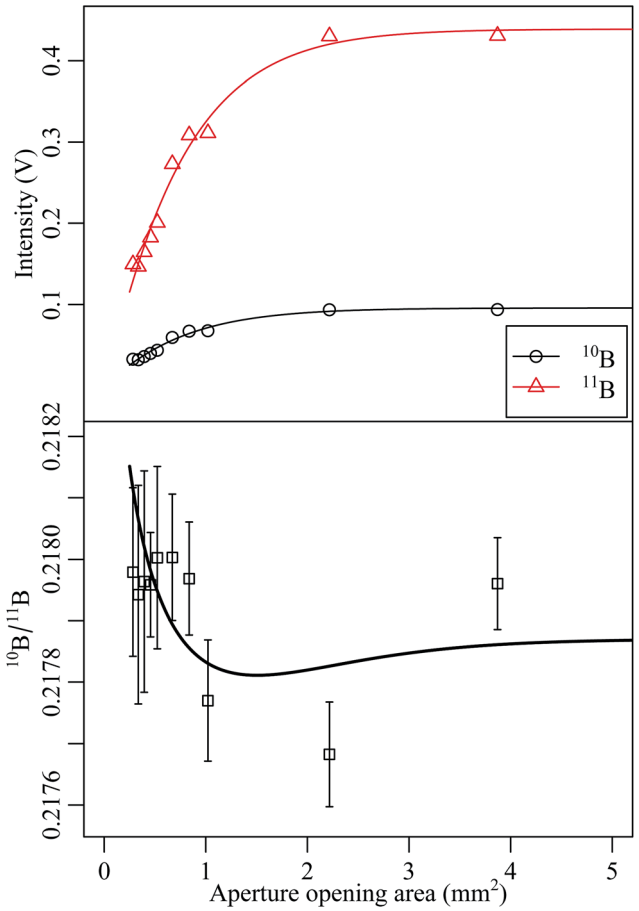

Fig. 4 Measured B intensity and fits of the respective data by a Weibull-distribution (top). The bottom part of the figure shows the measured ^{10}B/^{11}B isotope ratio as well as the quotient of the fit-functions.

of all measured isotopes of Pb, Cd and B was calculated to obtain the most representative dataset for the particular element. These datasets were subsequently fitted and for better comparability, the fits are normalized to the respective saturation intensities I_{sat}, as shown in Fig. 5. In a second step, the fit functions were differentiated. This was done for all three elements studied, the results for the deduced beam profiles are presented in Fig. 6. The beam profiles were assumed to be of Gaussian type. A correlation analysis supports this assumption, with correlation coefficients exceeding $R^2 \geq 0.99$. It should be noted that the measured datasets only provide data for radii greater than 0.25 mm, due to the aperture type applied. Therefore, the central part of the beam profile might not be represented by a Gaussian function correctly. For comparability reasons, the Gaussian functions obtained were normalized to the Gaussian integral (eqn (3)), with the peak height and width h and w, respectively.

$$\int_{-\infty}^{\infty} h e^{-(r/w)^2} dr = hw\sqrt{\pi} \quad (3)$$

From the fitted beam profiles, several characteristics were deduced, a list of such is given in Table 2. A direct comparison of the beam characteristics obtained to those described in the literature is difficult due the unique setups of the different experiments. However, a good agreement with the laser-excited

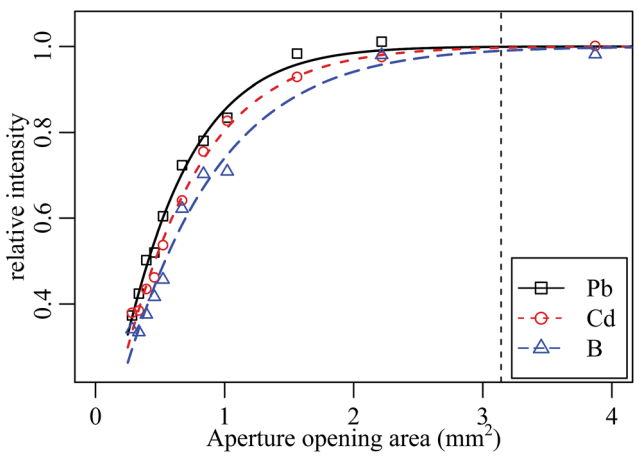

Fig. 5 Relative intensities for B, Cd and Pb including fits of the respective dataset by a Weibull-distribution. The vertical line indicates the orifice area of the standard system.

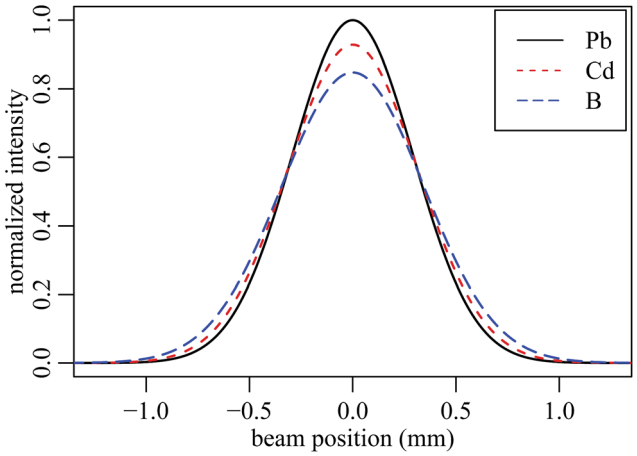

Fig. 6 Normalized beam profiles for B, Cd and Pb (Gaussian approximation).

Table 2 Ion beam characteristics at different peak heights (5% and 50%) and transmission yields for a standard Neptune MC-ICP-MS

Element	Width (5%)	Width (50%)	Transmission yield
B	1.68 mm	0.82 mm	99.6%
Cd	1.54 mm	0.74 mm	99.8%
Pb	1.44 mm	0.68 mm	99.9%

fluorescence profile shapes reported by Duersch and Farnsworth[20] is found, even though the authors did not apply any electric field behind the skimmer cone. These profiles show a Gaussian beam profile around 4 mm downstream of the skimmer tip, yet the beam width is much higher. The latter is attributed to the lack of an electric field, thus no focusing of the beam is expected. The data are also in good agreement with the beam profiles reported by Burgoyne *et al.*[18] In this article, the authors applied an electric field comparable to the field within the Neptune. However, the approach of ion implantation bears certain risks, as pointed out by Chen and Farnsworth.[17]

The transmission yield provided in Table 2 was calculated as the ratio of the Gaussian integral for a 2 mm aperture to the full beam. This is based on the fact that the standard instrument features a 2 mm fixed aperture. Therefore, it becomes clear that an almost full transmission of the ion beam is achieved in the standard setup. This statement has to be constrained to an ideal system, meaning that the ICP torch, the cones of the interface and the ion optics are perfectly aligned. Even small misalignments will introduce radial momenta on the ions, resulting in an off-axis beam, which in turn is partially blocked by the fixed aperture.

4 Conclusions

Based on the refined experimental setup compared to the ion implantation experiments,[14] the analytical conditions were matched to the concentration ranges usually applied and measurement times encountered in isotopic analysis. Even with these improvements, it was impossible to obtain evidence for a significant radial dependence of the boron isotopes within the ion beam. However, very valuable information on the beam intensity profiles could be gained. In particular, the beam width at the extraction lens aperture was almost identical to the aperture diameter in the standard instrument. From this, it can be concluded that space-charge effects and energy-selective ion transmission are of minor importance for mass discrimination once the ion beam is formed. Furthermore, the beam diameters are smaller than anticipated from visual observations of structural defects due to sputtering on the standard apertures, suggesting that the gross beam intensity is smaller than expected. The difference between visual observation and the actual ion beam width could be explained by the potential deposition of neutral species on the aperture, as suggested by Chen and Farnsworth.[17] The implication of a lower beam current has a large impact on space-charge considerations, since this effect is directly linked to the beam intensity. Typically the reported beam current in the range of several micro-amperes cannot be matched with the observation of a 2 mm beam width by ion beam modeling.[24] In order to simulate the very early ion extraction region of an ICP-MS instrument, it is of paramount importance to gain additional and reliable data on the transmitted ion beam current.

Acknowledgements

The support of the central workshop at the Paul Scherrer Institute, is highly appreciated. Additional support provided by Hans Leu and Andreas Spahr during the assembling is greatly acknowledged. Frank Vanhaecke acknowledges the Euramet – European Metrology Research Program (EMRP) and the European Union for the organizational research excellence grant (REG) provided in the context of the SIB09-Elements.

References

1 H. Longerich, B. Fryer and D. Strong, *Spectrochim. Acta, Part B*, 1987, **42**, 39–48.
2 M. Thirlwall, *Chem. Geol.*, 2002, **184**, 255–279.
3 J. Meija, L. Yang, R. Sturgeon and Z. Mester, *Anal. Chem.*, 2009, **81**, 6774–6778.
4 D. Porcelli and M. Baskaran, *Handbook of Environmental Isotope Geochemistry*, Springer Berlin Heidelberg, 2011, ch. 2, pp. 11–32.
5 C. Hawkesworth, *Mineral. Mag.*, 2005, **69**, 377–378.
6 L. Balcaen, L. Moens and F. Vanhaecke, *Spectrochim. Acta, Part B*, 2010, **65**, 769–786.
7 P. Vallelonga, P. Gabrielli, E. Balliana, A. Wegner, B. Delmonte, C. Turetta, G. Burton, F. Vanhaecke, K. Rosman, S. Hong, C. Boutron, P. Cescon and C. Barbante, *Quat. Sci. Rev.*, 2010, **29**, 247–255.
8 G. Rugel, T. Faestermann, K. Knie, G. Korschinek, M. Poutivtsev, D. Schumann, N. Kivel, I. Günther-Leopold,

R. Weinreich and M. Wohlmuther, *Phys. Rev. Lett.*, 2009, **103**, 072502.
9 G. Jörg, R. Bühnemann, S. Hollas, N. Kivel, K. Kossert, S. Van Winckel and C. L. v. Gostomski, *Appl. Radiat. Isot.*, 2010, **68**, 2339–2351.
10 Y. Nedjadi, C. Bailat, Y. Caffari, P. Froidevaux, C. Wastiel, N. Kivel, I. Günther-Leopold, G. Triscone, F. Jaquenod and F. Bochud, *Appl. Radiat. Isot.*, 2012, **70**, 1990–1996.
11 I. Günther-Leopold, N. Kivel, J. Kobler Waldis and B. Wernli, *Anal. Bioanal. Chem.*, 2008, **390**, 503–510.
12 G. H. Fontaine, B. Hattendorf, B. Bourdon and D. Günther, *J. Anal. At. Spectrom.*, 2009, **24**, 637–648.
13 N. Kivel, H.-D. Potthast, I. Günther-Leopold, F. Vanhaecke and D. Günther, *Spectrochim. Acta, Part B*, 2014, **93**, 34–40.
14 N. Kivel, I. Günther-Leopold, F. Vanhaecke and D. Günther, *Spectrochim. Acta, Part B*, 2012, **76**, 126–132.
15 G. Li, Y. Duan and G. M. Hieftje, *J. Mass Spectrom.*, 1995, **30**, 841–848.
16 X. Chen and R. Houk, *Spectrochim. Acta, Part B*, 1996, **51**, 41–54.
17 Y. Chen and P. B. Farnsworth, *Spectrochim. Acta, Part B*, 1997, **52**, 231–239.
18 T. W. Burgoyne, G. M. Hieftje and R. A. Hites, *Anal. Chem.*, 1997, **69**, 485–489.
19 B. S. Duersch, Y. Chen, A. Ciocan and P. B. Farnsworth, *Spectrochim. Acta, Part B*, 1998, **53**, 569–579.
20 B. S. Duersch and P. B. Farnsworth, *Spectrochim. Acta, Part B*, 1999, **54**, 545–555.
21 J. W. Olesik and M. P. Dziewatkoski, *J. Am. Soc. Mass Spectrom.*, 1996, **7**, 362–367.
22 I. I. Stewart and J. W. Olesik, *J. Am. Soc. Mass Spectrom.*, 1999, **10**, 159–174.
23 T. N. Olney, W. Chen and D. J. Douglas, *J. Anal. At. Spectrom.*, 1999, **14**, 9–17.
24 N. Kivel, H.-D. Potthast, I. Günther-Leopold, F. Vanhaecke and D. Günther, unpublished manuscript.